Thin Solid Films 682 (2019) 10–17

Contents lists available at ScienceDirect

Thin Solid Films

journal homepage: www.elsevier.com/locate/tsf

Magneto-optical effect in GaAs/GaAlAs semi-parabolic quantum well

Nguyen D. Hien[a,b], C.A. Duque[c], E. Feddi[d], Nguyen V. Hieu[e], Hoang D. Trien[e], Le T.T. Phuong[f], Bui D. Hoi[f], Le T. Hoa[f], Chuong V. Nguyen[g], Nguyen N. Hieu[h,*], Huynh V. Phuc[i,*]

[a] Laboratory of Magnetism and Magnetic Materials, Advanced Institute of Materials Science, Ton Duc Thang University, Ho Chi Minh City, Viet Nam
[b] Faculty of Applied Sciences, Ton Duc Thang University, Ho Chi Minh City, Viet Nam
[c] Grupo de Materia Condensada-UdeA, Instituto de Física, Facultad de Ciencias Exactas y Naturales, Universidad de Antioquia UdeA, Calle 70 No. 52-21, Medellín, Colombia
[d] LaMCScI, Group of Optoelectronic of Semiconductors and Nanomaterials, ENSET, Rabat, Mohammed V University in Rabat, Rabat, Morocco
[e] Department of Physics, University of Education, The University of Da Nang, Da Nang 550000, Viet Nam
[f] Center for Theoretical and Computational Physics, University of Education, Hue University, Hue 530000, Viet Nam
[g] Department of Materials Science and Engineering, Le Quy Don Technical University, Ha Noi 100000, Viet Nam
[h] Institute of Research and Development, Duy Tan University, Da Nang 550000, Viet Nam
[i] Division of Theoretical Physics, Dong Thap University, Cao Lanh 870000, Viet Nam

ARTICLE INFO

Keywords:
Semi-parabolic quantum well
Magneto-optical properties
Hydrostatic pressure
Temperature effects
Aluminum content

ABSTRACT

We theoretically study the combined effect of Al-concentration, hydrostatic pressure, and temperature on the magneto-optical absorption properties of a semi-parabolic quantum well (SPQW) by investigating the magneto-optical absorption coefficient (MOAC) and the full-width at half-maximum (FWHM). The expression of MOAC is expressed by the second-order golden rule approximation where the electron–longitudinal-optical (LO) phonon interaction is taken into account while the FWHM is obtained from the profile of the curves. The numerical calculations are made for a typical GaAs/GaAlAs quantum well. Our results showed that the Al-concentration, hydrostatic pressure, and temperature affect the magneto-optical absorption properties strongly. Threshold energy and the resonant peaks are non-monotonic functions of the Al-concentration. Moreover, it has been revealed that the magneto-optical absorption properties of SPQW can be controlled by changing these parameters.

1. Introduction

Because of their potential applications in the integrated optics, optical communications, as well as optoelectronic devices, the linear and nonlinear optical absorption in low-dimensional semiconductor systems have been extensively studied in recent decades [1–5]. Based on the framework of density matrix theory, Yesilgul et al. investigated the effects of externally applied intense laser, static electric and magnetic fields on the linear and nonlinear optical response in the asymmetric double quantum wells [1]. Shaaban and co-workers [2] have experimentally investigated the nonlinear refractive index and the absorption coefficient of co-doped ZnO thin films. The linear and nonlinear susceptibility and refractive index have also been experimentally observed in nanocrystalline Sn-doped ZnO thin films [3]. Darwish et al. [4] have experimentally studied the linear optical absorption coefficient and third-order nonlinear optical susceptibility in $GeSe_{2-\eta}Sn_{\eta}$ ($0 \leq \eta \leq 0.8$) thin films. The optical properties of the ZnAlO thin films have been experimentally investigated through studying the effect of Al-concentration on the intensity and transmittance [5]. However, in these works, the electron-phonon interaction and the combined effect of hydrostatic pressure and temperature were ignored. This is one of the main issues of our present study.

The combined effect of Al-concentration, hydrostatic pressure, and temperature has been demonstrated to be a simple and efficient way to modify and to run the electronic properties of low-dimensional semiconductor systems [6–8]. Using the $\mathbf{k}\cdot\mathbf{p}$ procedure, Reyes-Gómez et al. showed that the hydrostatic pressure and Al content affected strongly on the effective mass through the strong dependence of the different energy gap on these two external parameters [6]. Hermann and Weisbuch demonstrated, via a $\mathbf{k}\cdot\mathbf{p}$ perturbation theory, which provides the expressions of energies and wave functions in the vicinity of a semiconductor band extremum, that the effective mass is related to the k^2 term of the energy development [7]. Particularly, they found that near the $k = 0$ point, the conduction effective mass for a cubic semiconductor comes

* Corresponding authors.
E-mail addresses: nguyendinhhien@tdtu.edu.vn (N.D. Hien), hieunn@duytan.edu.vn (N.N. Hieu), hvphuc@dthu.edu.vn (H.V. Phuc).

https://doi.org/10.1016/j.tsf.2019.04.049
Received 8 September 2018; Received in revised form 3 April 2019; Accepted 29 April 2019
Available online 03 May 2019
0040-6090/

from the expansion $m^* = [1 + \Sigma_u(E_c - E_u)^{-1}|\langle S|p_x|u\rangle|^2]^{-1}m_0$, where m_0 is the free electron mass, S the conduction band wave function, u the state of energy E_u, and p_x is the x-component of the momentum operator. Also, they concluded that the dominant terms come from the interaction of the $\Gamma_1{}^c$ conduction band with the nearest bands of Γ_5 symmetry, i.e., the $\Gamma_5{}^v$ valence bands and the $\Gamma_5{}^c$, conduction bands. The lattice parameter of a cubic semiconductor can be modified by using hydrostatic pressure or changing the stoichiometry of the compound materials. Using, for instance, a first principle calculations it is possible to obtain the electronic structure of the perturbed system which finally provides the basic information to obtain the valence or conduction effective mass via a two bands $\mathbf{k}\cdot\mathbf{p}$ Hamiltonian. Also, based on the eight-band $\mathbf{k}\cdot\mathbf{p}$ Hamiltonian, Krishtopenko et al. [8] demonstrated that the change of hydrostatic pressure and temperature could be used for pushing transitions between topological insulator phases, band insulator, and semimetal. The effects of hydrostatic pressure on the exciton states [9] and the correlated electron-hole transition energy [10] have also been calculated in quantum wells. The effect of these parameters on the optical properties of the low-dimensional systems has been investigated [11–15]. According to the works, as mentioned earlier, the variation of these parameters affected either the magnitude or the position of resonant peaks. For example, the increasing hydrostatic pressure leads to the reduction in scale and the blue-shift feature of the absorption coefficient in quantum ring [11] and in quantum wire [12]. Whereas, an opposite result, i.e., the red-shift behavior, was reported via theoretical calculations in the zinc-blende GaN/InGaN quantum wells [13]. Besides, the red-shift response of the optical rectification coefficient was also obtained in the quantum well with an asymmetrical Gaussian structural potential [14] and in quantum dots [15]. This disagreement shows that the studying of the influence of these external parameters on the optical properties of such low-dimensional systems should be continued. In this work, we will demonstrate that in GaAs/GaAlAs semi-parabolic quantum well, the increase of the hydrostatic pressure results in the decrease of the threshold energy, leading to the red-shift behavior of the optical spectrum.

The precise control over both host and impurity atom profiles that is possible with Molecular Beam Epitaxy (MBE) techniques has accessed a new regime of heterojunction superlattice study [16]. A wide range of two-dimensional quantum well (QW) structures can be modeled with the MBE technique, among them: step-like QWs, parabolic and semi-parabolic QWs, and triangular QWs. It is well-known that when the symmetry of confinement potential of the systems is broken, the quantum confinement effect will enhance the electronic and optical properties of these systems. The triangular QW is the most typically asymmetrical 2D low dimensional system [16]. Also, the semi-parabolic quantum well (SPQW) is another kind of asymmetrical structure which has attracted the attention of many researchers in recent years [17–25]. The choice of parabolic potential profile is motivated by the experimental fact that the spectrum of single dots in GaAs is well described by a parabolic confinement potential [26,27]. In GaAs bulk material, the electron affinity is 4.07 eV, which corresponds to GaAs-vacuum interface [28]. Such kind of almost infinite confinement potential can be modeled via the infinite barrier at the extreme of the SPQW. To study the optical properties of this interesting model, many researchers have investigated the linear and nonlinear optical absorption coefficients [17–19], the optical rectification coefficients [20,21], as well as the second-order [22] and the third-order [23] susceptibilities. They demonstrated that the asymmetrical semi-parabolic confinement had more efficient to the optical properties in comparison with the regular parabolic ones [20,23]. This implies that the asymmetrical structural confinements have a significant effect on the optical properties of these types of the low-dimensional systems.

The goal of the present work is to study the combined effect of the Al-concentration, the hydrostatic pressure, and the temperature on the MOAC and FWHM in SPQW. To do this, in Sec. 2, we first present a brief of the electronic structure of SPQW in the presence of a perpendicular magnetic field. The expression of magneto-optical absorption coefficient is given in Sec. 3. In Sec. 4, we show our numerical results and discussion. Finally, our conclusions are shown in Sec. 5.

2. Electronic structure of SPQW in the presence of magnetic field

When a static magnetic field $\mathbf{B} = (0, 0, B)$ is applied to the GaAs/$Ga_{1-\eta}Al_\eta As$ SPQW grown along the z-axis, the one-electron Hamiltonian, under applied hydrostatic pressure (P) and temperature (T) for certain value of the Al-concentration (η), can be written as follows in the effective mass approximation

$$\mathcal{H} = \frac{(\mathbf{p} + e\mathbf{A})^2}{2m^*(\eta, P, T)} + U(z), \tag{1}$$

where $\mathbf{p}$ is the momentum operator of electron, e is the electron charge, $U(z)$ is the confinement potential in the z-direction given by [18,20,23].

$$U(z) = \begin{cases} m^*(\eta, P, T)\omega_z^2 z^2/2 & z \geq 0, \\ \infty & z < 0, \end{cases} \tag{2}$$

with ω_z being the frequency of the confining potential. In the above equations, $m^*(\eta, P, T)$ presents the electron effective mass, which is assumed to be dependent on η, P, and T, and can be expressed as [6,29,30].

$$\frac{m_0}{m^*(\eta, P, T)} = 1 + \frac{\xi(\eta)}{3}\left[\frac{2}{E_g^\Gamma(\eta, P, T)} + \frac{1}{E_g^\Gamma(\eta, P, T) + \Delta(\eta)}\right] + \zeta(\eta), \tag{3}$$

where m_0 is the free-electron mass, $\xi(\eta) = (28900 - 6290\eta)$ meV is the interband matrix element, $\Delta(\eta) = (314 - 66\eta)$ meV is the valence-band spin-orbit splitting, the parameter $\zeta(\eta) = -3.935 + 0.488\eta + 4.938\eta^2$ is related to the remote-band effects, and $E_g^\Gamma(\eta, P, T)$ is the energy gap function at Γ-point of the Brillouin zone given as

$$E_g^\Gamma(\eta, P, T) = a_1 + a_2\eta + a_3\eta^2 + \alpha_1 P - \frac{\beta_1 T^2}{T_0 + T}, \tag{4}$$

where $a_1 = 1519.4$ meV, $a_2 = 1360$ meV, $a_3 = 220$ meV, $\alpha_1 = 107$ meV/GPa, $\beta_1 = 0.5405$ meV/K, and $T_0 = 204$ K. In Eq. (4), the temperature dependence of the bandgap (last term on the right hand side) corresponds to the Varshni equation which describes the change in the energy bandgap of a semiconductor with temperature (T), where β_1 and T_0 are material specific constants [31]. Note that the $\xi(\eta)$ and $\Delta(\eta)$ parameters in Eq. (3) are obtained by linear interpolation between the corresponding parameters in GaAs and AlAs, whereas the $\zeta(\eta)$ parameter is obtained via a quadratic interpolation between them [6]. The same quadratic η-dependence has been used for the $Ga_{1-\eta}Al_\eta As$ bandgap. In the case of the hydrostatic pressure coefficient, α_1, the used value is obtained from experimental findings [6].

The electron wave-function and energy corresponding to the Hamiltonian in Eq. (1) have been already presented in Ref. [32], which was adapted from those in square quantum wells [33]. However, to be more convenient to follow we recall them as below in the Landau gauge of the vector potential $\mathbf{A} = (0, Bx, 0)$

$$|\alpha\rangle \equiv |N, n, k_y\rangle = (L_y)^{-1/2}\exp(ik_y y)\psi_N(x - x_0)\phi_n(z) \tag{5}$$

and

$$E_\alpha \equiv E_{N,n} = \left(N + \frac{1}{2}\right)\hbar\omega_c + \varepsilon_n. \tag{6}$$

Here, $N = 0,1,2, \ldots$ and n are respectively the Landau and electric subband quantum numbers, L_y and k_y are respectively the normalization length and the electron wave-vector in the y-direction, $\psi(x - x_0)$ is the normalized harmonic oscillator wave-function with $x_0 = -a_c{}^2 k_y$ being the center of the cyclotron orbit, $a_c = [\hbar/m^*(\eta, P, T)\omega_c]$ is the length radius of the orbit with $\omega_c = eB/m^*(\eta, P, T)$ being the cyclotron frequency. Note that, in this work, the influences of Al-concentration,

pressure, and temperature are taken into account. Also, the corresponding eigenfunction and eigenvalue in the z-direction are given by [18,20,23].

$$\phi_n(z) = A_n e^{-z^2/2a_z^2} H_{2n+1}\left(\frac{z}{a_z}\right), \tag{7}$$

$$\varepsilon_n = \left(2n + \frac{3}{2}\right)\hbar\omega_z, \quad n = 0,1,2, \ ..., \tag{8}$$

where $A_n = [2^{2n}(2n+1)!a_z\sqrt{\pi}]^{-1/2}$ is the normalization constant, $a_z = \{\hbar/[m^*(\eta,P,T)\omega_z]\}^{1/2}$ is the length radius of the orbit in the z-direction, and $H_{2n+1}(z/a_z)$ are the Hermite polynomials.

3. The expression of magneto-optical absorption coefficient

When considering the electron–longitudinal-optical (LO) phonon scattering, the MOAC is calculated through the transition probability for the photons absorption process [34].

$$K(\Omega) = \frac{1}{V_0(I/\hbar\Omega)} \sum_{\alpha,\alpha'} \mathscr{W}^{\pm}_{\alpha,\alpha} f_\alpha (1 - f_{\alpha'}), \tag{9}$$

where we follow the notation of Ref. [34], i.e., $I/\hbar\Omega$ is the average number of the incident photons per unit area per second with energy $\hbar\Omega$ and optical intensity $I = n_r c\varepsilon_0\Omega^2 {A_0}^2/2$, $V_0 = SL_z$ is the volume of the system with S being the area of the sample, and f_α and $f_{\alpha'}$ are the Fermi distribution functions of electron in the initial $|\alpha\rangle$ and final $|\alpha'\rangle$ states, respectively. The parameters ε_0, c, and A_0 are, respectively, the permittivity of vacuum, the speed of light in the vacuum, and the vector potential magnitude of the incident electromagnetic field, and $n_r = \sqrt{\chi_0(\eta,P,T)}$ is the refractive index, with $\chi_0(\eta,P,T)$ being the low-frequency dielectric constant, given below in Eq. (16). In Eq. (9), the sums are taken over all values of quantum numbers of the states $|\alpha\rangle$ and $|\alpha'\rangle$ excepted $\alpha = \alpha'$ due to the forbidden of self-absorption. The transition matrix element is given by the Born's second-order golden rule for the case of ℓ-photon absorption process [34]

$$\mathscr{W}^{\pm}_{\alpha,\alpha'} = \frac{2\pi}{\hbar} \sum_{\mathbf{q}} \sum_{\ell=1}^{\infty} (|\mathcal{M}^{\pm}_{\alpha,\alpha'}|^2 |\mathcal{M}^{\text{rad}}_{\alpha,\alpha'}|^2/\hbar^2\Omega^2) \times \frac{(\alpha_0 q)^{2\ell}}{(\ell!)^2 2^{2\ell}} \delta(E_{\alpha'} - E_\alpha - \ell\hbar\Omega \pm \hbar\omega_0), \tag{10}$$

$$|J_{NN'}(q_\perp)|^2 = \frac{N'!}{N!} e^{-u} u^{N'-N} [L_N^{N'-N}(u)]^2, \quad u = a_c^2 q_\perp^2/2, \tag{13}$$

$$\mathcal{F}_{nn'}(\pm q_z) = \int_0^{+\infty} \phi^*_{n'}(z) e^{\pm i q_z z} \phi_n(z) dz. \tag{14}$$

Here, $L_N^{N'-N}(u)$ are the associated Laguerre polynomials. The (η,P,T)-dependent high frequency dielectric constant, in Eq. (12), is [38].

$$\chi_\infty(\eta,P,T) = 10.89 - 2.73\eta. \tag{15}$$

And the low frequency static dielectric constant is expressed by [36,39].

$$\chi_0(\eta,P,T) = \chi_0(0,P,T) - 3.12\eta, \tag{16}$$

where [40–43].

$$\chi_0(0,P,T) = \begin{cases} \lambda_1 \exp[-\sigma P + \mu_1(T - T_1)], & T < 200 \text{ K}, \\ \lambda_2 \exp[-\sigma P + \mu_2(T - T_2)], & T \geq 200 \text{ K}, \end{cases} \tag{17}$$

where $\lambda_1 = 12.47$, $\lambda_2 = 13.18$, $\sigma = 1.73 \times 10^{-2}$ GPa^{-1}, $\mu_1 = 9.4 \times 10^{-5}$ K^{-1}, $\mu_2 = 20.4 \times 10^{-5}$ K^{-1}, $T_1 = 75.6$ K, and $T_2 = 300$ K.

In the steady-state, the matrix element for electron-photon interaction is given as follow through the dipole moment $e\mathscr{B}_{\alpha\alpha'} = e\langle\alpha'|\mathbf{r}|\alpha\rangle$ [44].

$$|\mathcal{M}^{\text{rad}}_{\alpha,\alpha'}|^2 = \frac{\Omega^2 A_0^2}{4} |\mathbf{n}\cdot e\mathscr{B}_{\alpha\alpha'}|^2, \tag{18}$$

where $\mathbf{n}$ is an unitary vector associated to the polarization of the incident electromagnetic field; in this work we assumed that the incident field is polarized along the x-direction ($\mathbf{n} = \mathbf{u}_x$). Using the eigenfunctions in Eq. (5), the magnitude of matrix element of the position operator in Eq. (18) yields

$$|\mathscr{B}_{\alpha\alpha'}| = [x_0\delta_{N',N} + (\alpha_c/\sqrt{2})(\sqrt{N}\delta_{N',N-1} + \sqrt{N+1}\delta_{N',N+1})]\delta_{k_{y'},k_y}. \tag{19}$$

The Eq. (19) implies that the magneto-optical transitions in SPQW satisfies the condition that the change of Landau level index by 0 or 1, i.e., $\Delta N = 0, \pm 1$. This is exactly consistent with that of the dipole type transitions in MoS_2 monolayer [34], graphene [45,46], and quantum well [47].

In the case of calculating up to the two-photon process, i.e., $\ell = 1, 2$, we thus obtain the following expression for the MOAC

$$K(\Omega) = \frac{S^2 e^4 \alpha_0^2 \chi^* \hbar\omega_0}{32\pi^2 n_r c\varepsilon_0^2 V_0 \alpha_c^6 \hbar^2\Omega} |J_{0,1}| \sum_{N,N'} |\mathscr{B}_{\alpha\alpha'}|^2 f_{N,0}(1 - f_{N',1}) \left\{ N_0^- \delta(X_1^-) + N_0^+ \delta(X_1^+) + \frac{\alpha_0^2}{8\alpha_c^2}(N + N' + 1)[N_0^- \delta(X_2^-) + N_0^+ \delta(X_2^+)] \right\}, \tag{20}$$

where $\mathbf{q} = (q_\perp, q_z)$ is the LO-phonon wave vector with ${q_\perp}^2 = {q_x}^2 + {q_y}^2$, the upper (+)/lower (−) sign refers to the phonons emission/absorption process, $\alpha_0 = (eF_0)/[m^*(\Omega^2 - {\omega_c}^2)]$ [35] is the dressing parameter with F_0 being the electric field strength of an electromagnetic field (F_0 is in the unit of V/m, and the α_0 is in the unit of m), and $\delta(\ldots)$ is the delta function. Note that although the expression of the transition matrix element presented here is similar with that in MoS_2 monolayer (see Eq. (12) of Ref. [34]), their distinguishing features are expressed through the electron–phonon matrix element $\mathscr{M}_{\alpha,\alpha,}{}^{\pm}$ given as follows in SPQW [32].

$$|\mathcal{M}^{\pm}_{\alpha,\alpha'}|^2 = |V(\mathbf{q})|^2 |J_{NN'}(q_\perp)|^2 |\mathcal{F}_{nn'}(\pm q_z)|^2 N_0^{\pm} \delta_{k_{y'},k_{y\pm q_y}}, \tag{11}$$

where $N_0{}^{\pm} = N_0 + 1/2 \pm 1/2$ with N_0 being the LO-phonon distribution function of energy $\hbar\omega_0 = (36.25 + 1.83\eta + 17.12\eta^2 - 5.11\eta^3)$ meV [36,37]. The other parameters in Eq. (11) are

$$|V(\mathbf{q})|^2 = \frac{4\pi e^2 \chi^* \hbar\omega_0}{\varepsilon_0 V_0 q^2}, \quad \chi^* = \left[\frac{1}{\chi_\infty(\eta,P,T)} - \frac{1}{\chi_0(\eta,P,T)}\right], \tag{12}$$

where the result is calculated for transition between two first-lowest states, i.e., $n = 0 \to n' = 1$, and

$$X_\ell^{\pm} = \Delta E \pm \hbar\omega_0 - \ell\hbar\Omega, \quad \ell = 1, 2, \tag{21}$$

where we have denoted $\Delta E = E_{N,\,1} - E_{N',\,0}$ is the threshold energy. In Eq. (20), $J_{0,\,1}$ is the overlap integral given as [32].

$$J_{0,1} = \int_{-\infty}^{+\infty} |\mathcal{F}_{01}(\pm q_z)|^2 dq_z = \frac{11\sqrt{\pi}}{4a_z\sqrt{2}}. \tag{22}$$

The expression of MOAC in Eq. (20) describes the transitions of electrons from $|0, 0\rangle$ state to $|1, 1\rangle$ state thanks to absorbed of one ($\ell = 1$) or two ($\ell = 2$) photons simultaneously absorbed or emitted an LO-phonon. In which, the delta functions imply the energy-momentum conservation law or also recalled the selection rules. Unfortunately, they will be divergent when their arguments equal to zero. To deal with this problem, we will replace these delta functions by the Lorentzians of width $\gamma^{\pm}$, namely $\delta(X_\ell{}^{\pm}) = (\gamma^{\pm}/\pi)[(X_\ell{}^{\pm})^2 + (\gamma^{\pm})^2]^{-1}$, with [33].

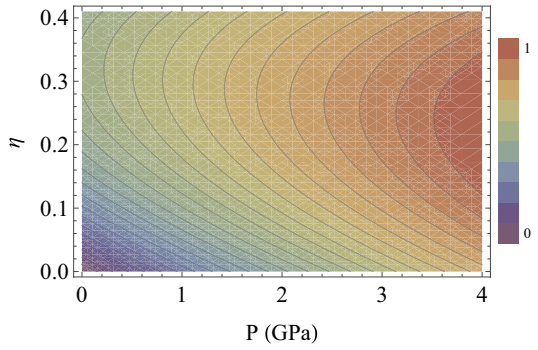

Fig. 1. Contour plot of the product $f_{0,\ 0}(1 - f_{1,\ 1})$ versus the Aluminum concentration (η) and hydrostatic pressure (P) at $T = 77$ K and $\hbar\omega_z/\hbar\omega_0 = 0.3$.

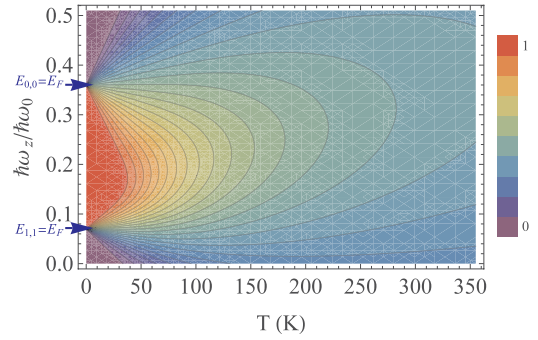

Fig. 2. Contour plot of the product $f_{0,\ 0}(1 - f_{1,\ 1})$ versus the ratio $\hbar\omega_z/\hbar\omega_0$ and temperature at $\eta = 0.3$ and $P = 2$ GPa.

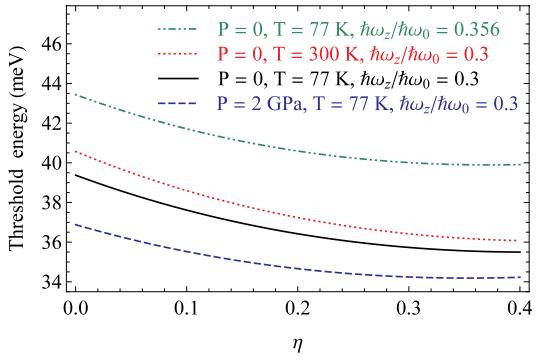

Fig. 3. Threshold energy as functions of Aluminum concentration for two different values of the ratio $\hbar\omega_z/\hbar\omega_0$, temperature, and hydrostatic pressure.

$$(\gamma^{\pm})^2 = \sum_{\mathbf{q}} |\mathcal{M}^{\pm}_{\alpha,\alpha'}|^2, \tag{23}$$

where the electron-phonon matrix element $\mathscr{M}_{\alpha,\ \alpha'}{}^{\pm}$ is shown in Eq. (11).

4. Numerical results and discussion

In this section, we will present our numerical results for the magneto-optical properties of GaAs/$Ga_{1-\eta}Al_\eta As$ SPQW through studying the MOAC and FWHM. To do this, we take $\alpha_0 = 15$ nm, $B = 10$ T, and $n_e = 3 \times 10^{16}$ cm^{-3} leading to the Fermi level energy $E_F = 26.15$ meV [32,36,48,49]. Here we assumed that the Fermi level energy does not depend on the Al-concentration, the pressure, and the temperature.

Because the product $f_{N,\ 0}(1 - f_{N',\ 1})$ has a strong effect on the magnitude of MOAC, in Figs. 1 and 2 we show the contour plot of the product $f_{0,\ 0}(1 - f_{1,\ 1})$, which presents the interband transition between the ground ($N = 0, n = 0$) and the first excited ($N' = 1, n' = 1$) states. From Fig. 1 we can see that this product is an increasing function of P while its dependence on η is very complex. When η increase (P is fixed), this product increases up to the maximum value around $\eta = 0.34$ for $P = 0$, then it starts reducing if the Al-concentration is more increased.

Fig. 2 shows the contour plot of the product $f_{0,\ 0}(1 - f_{1,\ 1})$ versus the ratio $\hbar\omega_z/\hbar\omega_0$ and temperature at $\eta = 0.3$ and $P = 2$ GPa. Although the electron–LO-phonon interaction plays only the primary role in the high-temperature region, to clarify the issue, we would like to show here in a large interval of temperature even down to a very low value. It can be seen from the figure that all contours tend to converge to two points located at $\hbar\omega_z/\hbar\omega_0 = 0.066$ and 0.356 with $T \to 0$ K. At these two points, the first excited ($E_{1,\ 1}$) and the ground state energies ($E_{0,\ 0}$) equal to Fermi level energy, respectively. Therefore, at the very low-temperature region, the best interval of the values of ratio $\hbar\omega_z/\hbar\omega_0$ is between these two values. At the higher value of temperature, this interval is broader, and the product $f_{0,\ 0}(1 - f_{1,\ 1})$ decreases due to the thermal spreading of the Fermi distribution functions.

In Fig. 3, we show the threshold energy as functions of the Al-concentration for two values of the ratio $\hbar\omega_z/\hbar\omega_0$, temperature, and the hydrostatic pressure. The threshold energy presented here is $\Delta E = E_{1,\ 1} - E_{0,\ 0}$, standing for the transition between ground and the first excited states. The solid line (black) is for $P = 0$, $T = 77$ K and $\hbar\omega_z/\hbar\omega_0 = 0.3$. In comparison with the solid line, in each of the other lines, there is only one parameter changed while other ones are kept fixed. In contrast to the other systems such as quantum rings [30] and quantum wells [38], in the present work, the threshold energy is not a monotonous function of η. For example, for the dashed blue line ($P = 2$ GPa, $T = 77$ K, $\hbar\omega_z/\hbar\omega_0 = 0.3$), firstly, ΔE decreases with the Al-concentration, reaching the minimum value of 34.19 meV at $\eta = 0.35$, and then it increases when the Al-concentration continuously increases. The complexity arising here is because we have considered the dependence of phonon energy on η. We can easily deduce from Eq. (6) that ΔE depends on η through the electron effective mass m^* and the confinement energy $\hbar\omega_z$, which depends on η through the ratio of $\hbar\omega_z/\hbar\omega_0 = 0.3$. When η increases, there will be two competitive processes: while the electron effective mass increases resulting in the decrease of the threshold energy, the confinement energy increases (to ensure the ratio of $\hbar\omega_z/\hbar\omega_0 = 0.3$, because $\hbar\omega_0$ is an increasing function of η) resulting in the increase of the threshold energy. The result is shown in Fig. 3 implies that in the small values of η the mass-increasing effect is predominant, while the effect of the increasing confinement energy seems to dominate at the higher values of η. Besides, the effect of the ratio of $\hbar\omega_z/\hbar\omega_0$, the temperature, and the hydrostatic pressure on the threshold energy is also clearly illustrated in this figure: ΔE increases with the ratio of $\hbar\omega_z/\hbar\omega_0$ and temperature but decreases with the hydrostatic pressure.

Fig. 4 describes MOAC as functions of the incident photon energy for three different values of η. It is easy to see two resonant peaks in each curve corresponding to the one-photon ($\ell = 1$) and the two-photon ($\ell = 2$) absorption processes. For example, the solid line stands for $\eta = 0$, corresponding to threshold energy $\Delta E = 37.14$ meV, having the one- and two-photon resonant peaks at $\hbar\Omega = 73.39$ meV and 36.70 meV, respectively. These two peaks satisfy the selection rule

$$\ell\hbar\Omega = \Delta E + \hbar\omega_0, \quad \ell = 1, 2, \tag{24}$$

describing the fact that an electron at the ground state absorbs one ($\ell = 1$) or two ($\ell = 2$) photons and simultaneously emits one LO-phonon to transfer to the first excited state.

Note that the processes with both phonon emission and phonon absorption might happen as shown in Eqs. (20) and (21). However, in this work, only the phonon emission process is observed while the phonon absorption one is disappeared, which can be explained as

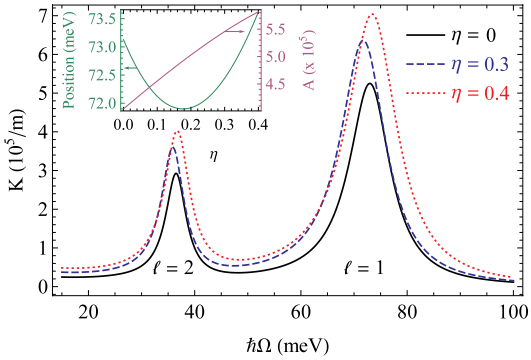

Fig. 4. MOAC as functions of incident photon energy for there different values of the Aluminum concentration at $P = 2$ GPa, $T = 77$ K, and $\hbar\omega_z/\hbar\omega_0 = 0.3$. The inset illustrates the position of one-photon peak ($\ell = 1$, left vertical axis) and the product $A = \chi^* |J_{0,1}| f_{0,0}(1 - f_{1,1})$ (right vertical axis) as functions of η.

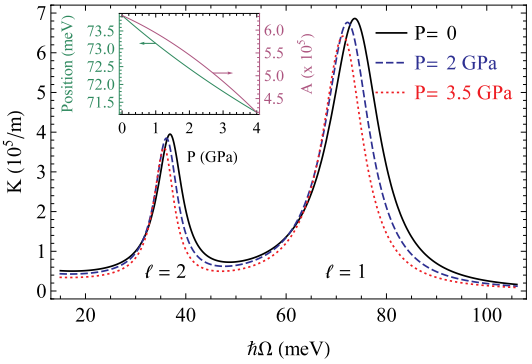

Fig. 6. MOAC as functions of the photon energy for there different values of the hydrostatic pressure at $\eta = 0.3$, $T = 77$ K, and $\hbar\omega_z/\hbar\omega_0 = 0.3$. The inset illustrates the position of one-photon peak ($\ell = 1$, left vertical axis) and the product $A = \chi^* |J_{0,1}| f_{0,0}(1 - f_{1,1})$ (right vertical axis) as functions of P.

follows: The absorbed photon energy along with the phonon absorption must satisfy the selection rule: $\ell\hbar\Omega = \Delta E - \hbar\omega_0$, $(\ell = 1, 2)$. For the chosen values of the input parameters ($P = 2$ GPa, $T = 77$ K, $\hbar\omega_z/\hbar\omega_0 = 0.3$), the corresponding energies of absorbed photons are: $\ell\hbar\Omega = 0.63$ meV for $\eta = 0$, while for the two other cases ($\eta = 0.3$ and 0.4) the absorbed photon energies will have negative values because the threshold energy (ΔE) is smaller than the LO-phonon energy ($\hbar\omega_0$), therefore, these two cases can not happen. Although the phonon absorption process does happen in the case of $\eta = 0$, the energy of the absorbed photon is so small, nearly coincide with the singularity point ($\hbar\Omega = 0$). That is the reason why, in this work, the resonant peaks due to the phonon absorption have not been observed. Note that, this feature only happens for the SPQW, where the threshold energy is small. In other models of quantum well [50,51], both phonon emission and absorption processes are normally observed.

Besides, unlike in the square quantum well [38], the dependence of the peaks position here is more complicated. With the increasing Al-concentration, first, the resonant peaks shift toward the low-energy side and then turn to the higher region of energy. This can explain from the dependence of the peaks position on the Al-concentration as shown in the inset (left vertical axis), in which the physical meaning can be derived from the dominant effect of the increasing LO-phonon energy in comparison with the mass-increasing effect, similarly to what happened with the threshold energy shown in Fig. 3. Moreover, the increase of the magnitude of MOAC with the increasing Al-concentration results from the rise of product $A = \chi^* |J_{0,1}| f_{0,0}(1 - f_{1,1})$ as shown in the inset (right vertical axis). This can be explained from the increase of the reduced dielectric constant χ^* and the overlap integral J_{01} with the increasing Al-concentration. In which the increase of J_{01} with η reveals that the overlap between the ground state and first excited state increases when the Al-concentration increases.

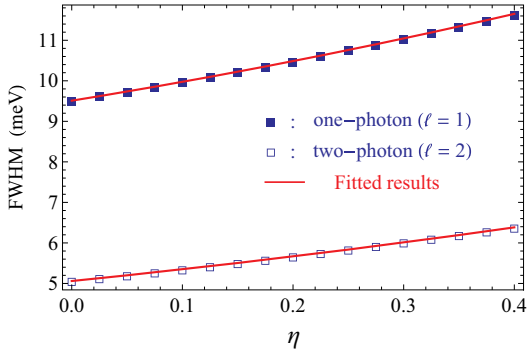

Fig. 5. FWHM as functions of the Aluminum concentration at $P = 2$ GPa, $T = 77$ K, and $\hbar\omega_z/\hbar\omega_0 = 0.3$.

The dependence of the FWHM on the Al-concentration is shown in Fig. 5 for both one- and two-photon absorption processes. It is found that FWHM is the nonlinearly increasing function of η and they can be expressed as the following fitted results: FWHM (meV) $= 9.51 + 4.41\eta + 2.36\eta^2$ for the one-photon process and FWHM (meV) $= 5.06 + 2.77\eta + 1.35\eta^2$ for the two-photon ones, respectively, which are illustrated by the solid (red) lines. Although at present, there is no experimental data to support our results, we hope that these prediction values of the FWHM will be useful data for the experimental investigation in the future. Besides, because the FWHM is closely associated with electron-phonon scattering, the increase of FWHM with the Al-concentration implies that the electron-phonon interaction will be enhanced when the effect of the Al-concentration is included. This result is in agreement with previous findings reported in the square [38] and the parabolic [52] quantum wells. All of these works showed that when the Al-concentration increases, the electron–phonon interaction increases, leading to the increase of the FWHM.

In Fig. 6, the MOAC is shown as functions of the photon energy for several values of hydrostatic pressure. It is well-known that when the hydrostatic pressure increases, there will be a crossover from Γ to X points [6,53]. Considering a GaAs/$Ga_{1-\eta}Al_\eta As$ QW under hydrostatic pressure, it is known that for $\eta = 0.3$, $T = 77$ K, and $P_1 = 0.91$ GPa there is a crossover between the Γ and X minima in the $Ga_{0.7}Al_{0.3}As$ barrier material, whereas at $P_2 = 4.46$ GPa the crossover occurs between the X minimum of the $Ga_{0.7}Al_{0.3}As$ barrier material and the Γ minimum of the GaAs well material. As the hydrostatic pressure increases the following behavior is observed for a confined electron in the heterostructure: *i*) in the range of $0 \le P \le P_1$, the potential barrier height remains constant and the changes of the energy levels are associated mainly to variations in the effective mass, *ii*) for $P_1 \le P \le P_2$ there is a monotonous reduction of the barrier height which effect is additive to those of the effective mass, and finally *iii*) for $P > P_2$ there is a semiconductor-semimetal transition and the electron loses its confinement. We have to stress that the effects of the $\Gamma - X$ mixing induced by hydrostatic pressure can be taken into account by considering a position dependent effective mass. This subject can motivate further research and will be reported elsewhere. In this work, the MOAC is calculated for transitions at the Γ-point of the Brillouin zone; therefore we will not take into account the effect of crossover Γ-X induced by pressure. We can see from the figure that when the hydrostatic pressure increases, the decrease of the peaks' position as shown in the inset (left vertical axis) leads to the red-shift behavior of the MOAC. Meanwhile, the decrease of the product $A = \chi^* |J_{0,1}| f_{0,0}(1 - f_{1,1})$ (right vertical axis) results in the reduction of the magnitude of MOAC. This is completely consistent with that reported in parabolic quantum

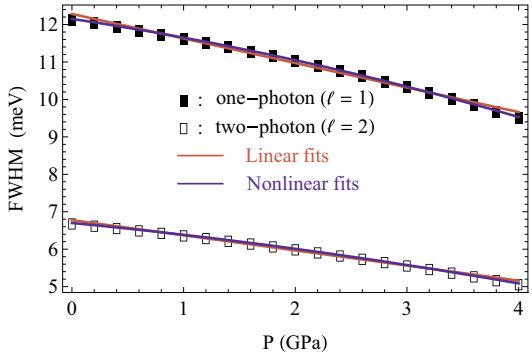

Fig. 7. FWHM as functions of the hydrostatic pressure at $\eta = 0.3$, $T = 77$ K, and $\hbar\omega_z/\hbar\omega_0 = 0.3$.

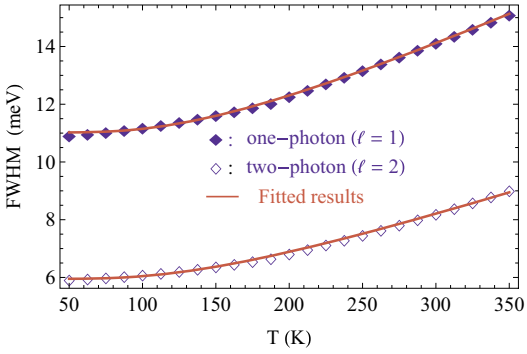

Fig. 9. FWHM as functions of the temperature at $\eta = 0.3$, $P = 2$ GPa, and $\hbar\omega_z/\hbar\omega_0 = 0.3$.

well [52] as well as in the other low-dimensional systems [38,40,48,54,55]. The red-shift phenomenon can be physically explained by the reduction of the threshold energy with the increasing hydrostatic pressure as shown in Fig. 3.

The result in Fig. 7 indicates that FWHM is approximately a linearly decreasing function of hydrostatic pressure. The best linear fits found are

$$\text{FWHM (meV)} = \alpha_P + \beta_P P, \tag{25}$$

where $\alpha_P = 12.27$ meV(7.048 meV) and $\beta_P = -0.65$ meVGPa^{-1} (-0.44 meVGPa^{-1}) for the one- (two-) photon absorption process (with P in GPa), respectively, which are presented by the solid red lines in Fig. 7. To be more accurate, we can also describe FWHM as nonlinear functions of P as follows

$$\text{FWHM (meV)} = \gamma_P + \delta_P P + \varepsilon_P P^2, \tag{26}$$

where $\gamma_P = 12.142$ meV (6.970 meV), $\delta_P = -0.445$ meVGPa^{-1} (-0.315 meVGPa^{-1}), and $\varepsilon_P = -0.052$ meVGPa^{-2} (-0.031 meVGPa^{-2}) for the one- (two-) photon absorption process, respectively, which are shown by the solid blue lines. It is clear that although the nonlinear fitted results describe more accurately, their expressions are more complicated as compared to linear cases. Therefore, in this case, the linear fits are good enough to describe the obtained results. Besides, the obtained result that FWHM decreases with the decreasing hydrostatic pressure is consistent with previous works [38,52].

Fig. 8 shows the dependence of MOAC on the photon energy for three different values of the temperature. It is observed that when the temperature increases the MOAC shows a slight blue-shift feature of the peaks' position and a reduction in the magnitude. These results are consistent with previous works [38,52,54,56]. The causes of these results can be explained as follows: the blue-shift behavior of the MOAC is the result of the increase of the threshold energy with temperature (see Fig. 3), which is also clearly described by the increase of the peaks position as shown in the inset (left vertical axis). Meanwhile, the decrease of the MOAC's magnitude results from the decrease of the product $A = \chi^* |J_{0,1}| f_{0,0}(1 - f_{1,1})$ (right vertical axis of the inset). Besides, we can also see from the inset that the product A rapidly decreases in the interval of temperature from $T = 50$ K to $T = 200$ K, then the product A is almost unchanged in the range of temperature $T > 200$ K. These features of the product A are illustrated by the change of the magnitude of MOAC as shown in Fig. 8. Moreover, the unusual feature of the product A at $T = 200$ K (shown in the inset) is derived from the expression of $\chi_0(0, P, T)$ as shown in Eq. (17). It is noted that although the MOAC's magnitudes are almost maintained in the interval $T > 200$ K, the width of their resonant peaks is broadened by the temperature. The influence of temperature on the width of resonant peaks (or FWHM) will be discussed in more details in Fig. 9.

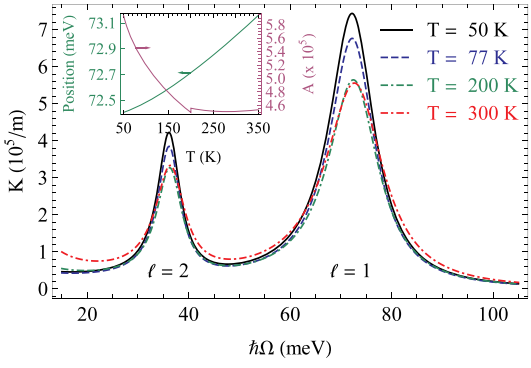

Fig. 8. MOAC as functions of the photon energy for there different values of the temperature at $\eta = 0.3$, $P = 2$ GPa, and $\hbar\omega_z/\hbar\omega_0 = 0.3$. The inset illustrates the position of one-photon peak ($\ell = 1$, left vertical axis) and the product $A = \chi^* |J_{0,1}| f_{0,0}(1 - f_{1,1})$ (right vertical axis) as functions of T.

Finally, the dependence of FWHM on temperature is shown in Fig. 9. It is well-known that the thermal broadening FWHM caused by the electron-LO-phonon can be expressed as follows [57].

$$\text{FWHM}[\text{meV}] = \gamma_0 + \gamma_1 N_0(T[\text{K}]), \tag{27}$$

where $N_0(T) = [e^{\hbar\omega_0/k_B T} - 1]^{-1}$ is the LO-phonon distribution function with k_B being the Boltzmann constant. Using this expression, we found the best fits as follows for the low-temperature part, γ_0, and the thermal broadening part, γ_1, of FWHM: $\gamma_0 = 11.02$ (5.95) and $\gamma_1 = 10.43$ (7.62) corresponding to the one- (two-) photon process. These fitted results are illustrated by the solid red lines in Fig. 9, in which the fitted consequence for the one-photon process is significantly consistent with the experimental result reported in GaAs/$Al_{0.3}Ga_{0.7}$As quantum wells, i.e., $\eta = 0.3$ [57].

5. Conclusion

In summary, we have studied the combined effect of Aluminum concentration, hydrostatic pressure, and temperature on the magneto-optical absorption properties of the GaAs/GaAlAs SPQW by examining in detail the dependence of threshold energy, MOAC, and FWHM on these parameters. The results show that the threshold energy is a non-monotonic function of Al-concentration, increase with the temperature, and decreases with the pressure.

The present results also show a significant dependence of MOAC on the Al-concentration, the pressure, and the temperature. The magnitude of MOACs increases with Al-concentration but decreases with pressure and temperature. The position of MOACs' peaks is a non-monotonic function of Al-concentration, but they give the red-shift with the pressure and slight blue-shift with the temperature.

Our results also indicate that the FWHM is strongly influenced by these parameters in both processes: one- and two-photon cases. FWHM

is a nonlinearly increasing function of Al-concentration, almost a linearly decreasing function of pressure, and depends on the temperature with an exponential function. We hope that our specific results about the FWHM might be useful data for the experimental observation in the future.

Acknowledgments

This research was funded by Ministry of Education and Training of Vietnam under Grant number B2019-DNA-07. C.A.D. is grateful to the Colombian Agencies: CODI-Universidad de Antioquia (Estrategia de Sostenibilidad de la Universidad de Antioquia and projects "Propiedades magneto-ópticas y óptica no lineal en superredes de Grafeno" and "Estudio de propiedades ópticas en sistemas semiconductores de dimensiones nanoscópicas"), and Facultad de Ciencias Exactas y Naturales-Universidad de Antioquia (CAD exclusive dedication projects 2018-2019).

References

[1] U. Yesilgul, E.B. Al, J.C. Martínez-Orozco, R.L. Restrepo, M.E. Mora-Ramos, C.A. Duque, F. Ungan, E. Kasapoglu, Linear and nonlinear optical properties in an asymmetric double quantum well under intense laser field: effects of applied electric and magnetic fields, Opt. Mater. 58 (2016) 107.
[2] E.R. Shaaban, M. El-Hagary, E.S. Moustafa, H.S. Hassan, Y.A.M. Ismail, M. Emam-Ismail, A.S. Ali, Structural, linear and nonlinear optical properties of co-doped ZnO thin films, Appl. Phys. A Mater. Sci. Process. 122 (2016) 20.
[3] V. Ganesh, I. Yahia, S. AlFaify, M. Shkir, Sn-doped zno nanocrystalline thin films with enhanced linear and nonlinear optical properties for optoelectronic applications, J. Phys. Chem. Solids 100 (2017) 115.
[4] A. Darwish, M. Rashad, A. Bekheet, M. El-Nahass, Linear and nonlinear optical properties of $GeSe_{2-x}Sn_x$ thin films for optoelectronic applications, J. Alloys Compd. 709 (2017) 640.
[5] G.P. Bharti, A. Khare, Structural and linear and nonlinear optical properties of $Zn_{1-x}Al_xO$ ($0 \le x \le 0.10$) thin films fabricated via pulsed laser deposition technique, Opt. Mater. Express 6 (2016) 2063.
[6] E. Reyes-Gómez, N. Raigoza, L.E. Oliveira, Effects of hydrostatic pressure and aluminum concentration on the conduction-electron g factor in GaAs-(Ga,Al)As quantum wells under in-plane magnetic fields, Phys. Rev. B 77 (2008) 115308.
[7] C. Hermann, C. Weisbuch, $\mathbf{k}\cdot\mathbf{p}$ perturbation theory in III-V compounds and alloys: a reexamination, Phys. Rev. B 15 (1977) 823.
[8] S.S. Krishtopenko, I. Yahniuk, D.B. But, V.I. Gavrilenko, W. Knap, F. Teppe, Pressure- and temperature-driven phase transitions in HgTe quantum wells, Phys. Rev. B 94 (2016) 245402.
[9] N. Raigoza, E. Reyes-Gómez, C.A. Duque, L.E. Oliveira, Hydrostatic pressure and growth-direction magnetic field effects on the exciton states in coupled GaAs-(Ga, Al)As quantum wells, J. Phys. Condens. Matter 19 (2007) 256202.
[10] N. Raigoza, C.A. Duque, E. Reyes-Gómez, L.E. Oliveira, Hydrostatic-pressure effects on the correlated electronhole transition energies in GaAs-$Ga_{1x}Al_xAs$ semiconductor quantum wells, Phys. Status Solidi B 243 (2006) 635.
[11] R.L. Restrepo, M.G. Barseghyan, M.E. Mora-Ramos, C.A. Duque, Effects of hydrostatic pressure on the nonlinear optical properties of a donor impurity in a GaAs quantum ring, Phys. E. 51 (2013) 48.
[12] M. Santhi, A. John Peter, C. Yoo, Hydrostatic pressure on optical absorption and refractive index changes of a shallow hydrogenic impurity in a GaAs/GaAlAs quantum wire, Superlattice. Microst. 52 (2012) 234.
[13] C.M. Duque, A.L. Morales, M.E. Mora-Ramos, C.A. Duque, Exciton-related optical properties in zinc-blende GaN/InGaN quantum wells under hydrostatic pressure, Phys. Status Solidi B 252 (2015) 670.
[14] X. Liu, L. Zou, C. Liu, Z.-H. Zhang, J.-H. Yuan, The nonlinear optical rectification and second harmonic generation in asymmetrical Gaussian potential quantum well: effects of hydrostatic pressure, temperature and magnetic field, Opt. Mater. 53 (2016) 218.
[15] R. Ben Mahrsia, M. Choubani, L. Bouzaiene, H. Maaref, Nonlinear optical rectification in a vertically coupled lens-shaped InAs/GaAs quantum dots with wetting layers under hydrostatic pressure and temperature, J. Alloys Compd. 671 (2016) 200.
[16] R. Dingle, H.L. Störmer, A.C. Gossard, W. Wiegmann, Electronic properties of the GaAs-AlGaAs interface with applications to multi-interface heterojunction superlattices, Surf. Sci. 98 (1980) 90.
[17] Z. Li, Calculation of linear and nonlinear intersubband optical absorptions in electric-field-biased semiparabolic quantum wells, Opt. Quant. Electron. 36 (2004) 665.
[18] X. Yu, Y. Yu, Optical absorptions in asymmetrical semi-parabolic quantum wells, Superlattice. Microst. 62 (2013) 225.
[19] C.-J. Zhang, K.-X. Guo, Polaron effects on the optical absorptions in asymmetrical semi-parabolic quantum wells, Phys. E. 39 (2007) 103.
[20] C.-J. Zhang, K.-X. Guo, Polaron effects on the optical rectification in asymmetrical semi-parabolic quantum wells, Physica B 387 (2007) 276.
[21] M. Karimi, A. Keshavarz, G. Rezaei, Optical rectification and second harmonic generation of finite and infinite semi-parabolic quantum wells, J. Comput. Theor. Nanosci. 8 (2011) 1340.
[22] C.-J. Zhang, K.-X. Guo, Polaron effects on the second-order susceptibilities in asymmetrical semi-parabolic quantum wells, Phys. E. 33 (2006) 363.
[23] C.-J. Zhang, K.-X. Guo, Polaron effects on the third-order nonlinear optical susceptibility in asymmetrical semi-parabolic quantum wells, Physica B 383 (2006) 183.
[24] N.T. Tien, N.T.N. Hung, T.T. Nguyen, P.T.B. Thao, Linear intersubband optical absorption in the semiparabolic quantum wells based on AlN/AlGaN/AlN under a uniform electric field, Physica B 519 (2017) 63.
[25] R.-Y. Yan, J. Tang, Z.-H. Zhang, Optical properties in GaAs/AlGaAs semiparabolic quantum wells by the finite difference method: combined effects of electric field and magnetic field, Int. J. Mod. Phys. B 32 (2018) 1850159.
[26] S. Tarucha, D.G. Austing, T. Honda, R.J. van der Hage, L.P. Kouwenhoven, Shell filling and spin effects in a few electron quantum dot, Phys. Rev. Lett. 77 (1996) 3613.
[27] G. Burkard, D. Loss, D.P. DiVincenzo, Coupled quantum dots as quantum gates, Phys. Rev. B 59 (1999) 2070.
[28] S.M. Sze, Physics of Semiconductor Devices, 2nd edition, Wiley-Interscience, New York, 1981, p. 878.
[29] I.A. Yugova, A. Greilich, D.R. Yakovlev, A.A. Kiselev, M. Bayer, V.V. Petrov, Y.K. Dolgikh, D. Reuter, A.D. Wieck, Universal behavior of the electron g factor in GaAs/Al_xGa_{1-x}as quantum wells, Phys. Rev. B 75 (2007) 245302.
[30] H.M. Baghramyan, M.G. Barseghyan, A.A. Kirakosyan, R.L. Restrepo, C.A. Duque, Linear and nonlinear optical absorption coefficients in GaAs/$Ga_{1-x}Al_x$as concentric double quantum rings: effects of hydrostatic pressure and aluminum concentration, J. Lumin. 134 (2013) 594.
[31] E. Grilli, M. Guzzi, R. Zamboni, L. Pavesi, High-precision determination of the temperature dependence of the fundamental energy gap in Gallium Arsenide, Phys. Rev. B 45 (1992) 1638.
[32] L.V. Tung, H.V. Phuc, Nonlinear optical absorption via two-photon process in asymmetrical semi-parabolic quantum wells, Superlattice. Microst. 89 (2016) 288.
[33] M.P. Chaubey, C.M. Van Vliet, Transverse magnetoconductivity of quasi-two-dimensional semiconductor layers in the presence of phonon scattering, Phys. Rev. B 33 (1986) 5617.
[34] C.V. Nguyen, N.N. Hieu, N.A. Poklonski, V.V. Ilyasov, L. Dinh, T.C. Phong, L.V. Tung, H.V. Phuc, Magneto-optical transport properties of monolayer MoS_2 on polar substrates, Phys. Rev. B 96 (2017) 125411.
[35] W. Xu, R.A. Lewis, P.M. Koenraad, C.J.G.M. Langerak, High-field magnetotransport in a two-dimensional electron gas in quantizing magnetic fields and intense terahertz laser fields, J. Phys. Condens. Matter 16 (2004) 89.
[36] S. Adachi, GaAs, AlAs, and Al_xGa_{1-x}as: material parameters for use in research and device applications, J. Appl. Phys. 58 (1985) R1.
[37] J. Gong, X.X. Liang, S.L. Ban, Confined LO-phonon assisted tunneling in a parabolic quantum well with double barriers, J. Appl. Phys. 100 (2006) 023707.
[38] H.V. Phuc, Nonlinear optical absorption via two-photon process in GaAs/$Ga_{1-x}al_x$as quantum well, J. Phys. Chem. Solids 82 (2015) 36.
[39] G.A. Samara, Temperature and pressure dependences of the dielectric constants of semiconductors, Phys. Rev. B 27 (1983) 3494.
[40] M. Nazari, M.J. Karimi, A. Keshavarz, Linear and nonlinear optical absorption coefficients and refractive index changes in modulation-doped quantum wells: effects of the magnetic field and hydrostatic pressure, Physica B 428 (2013) 30.
[41] M. Karimi, G. Rezaei, M. Nazari, Linear and nonlinear optical properties of multilayered spherical quantum dots: effects of geometrical size, hydrogenic impurity, hydrostatic pressure and temperature, J. Lumin. 145 (2014) 55.
[42] E. Li, Material parameters of InGaAsP and InAlGaAs systems for use in quantum well structures at low and room temperatures, Phys. E. 5 (2000) 215.
[43] E. Kasapoglu, F. Ungan, H. Sari, I. Sökmen, The hydrostatic pressure and temperature effects on donor impurities in cylindrical quantum wire under the magnetic field, Phys. E. 42 (2010) 1623.
[44] S.L. Chuang, Physics of Optoelectronic Devices, Wiley, New York, 1995.
[45] V. Gusynin, S. Sharapov, J. Carbotte, Anomalous absorption line in the magneto-optical response of graphene, Phys. Rev. Lett. 98 (2007) 157402.
[46] M. Koshino, T. Ando, Magneto-optical properties of multilayer graphene, Phys. Rev. B 77 (2008) 115313.
[47] H.V. Phuc, N.D. Hien, L. Dinh, T.C. Phong, Confined optical-phonon-assisted cyclotron resonance in quantum wells via two-photon absorption process, Superlattice. Microst. 94 (2016) 51.
[48] F. Ungan, U. Yesilgul, S. Sakiroglu, M.E. Mora-Ramos, C.A. Duque, E. Kasapoglu, H. Sari, I. Sökmen, Simultaneous effects of hydrostatic pressure and temperature on the nonlinear optical properties in a parabolic quantum well under the intense laser field, Opt. Commun. 309 (2013) 158.
[49] H.V. Phuc, L. Van Tung, Linear and nonlinear phonon-assisted cyclotron resonances in parabolic quantum well under the applied electric field, Superlattice. Microst. 71 (2014) 124.
[50] K.D. Pham, L. Dinh, P.T. Vinh, C.A. Duque, H.V. Phuc, C.V. Nguyen, LO-phonon-assisted cyclotron resonance in a special asymmetric hyperbolic-type quantum well, Superlattice. Microst. 120 (2018) 738.
[51] K.D. Pham, N.N. Hieu, L.T.T. Phuong, B.D. Hoi, C.V. Nguyen, H.V. Phuc, Phonon 'assisted cyclotron resonance in special symmetric quantum wells, Appl. Phys. A Mater. Sci. Process. 124 (2018) 656.
[52] T.C. Phong, H.V. Phuc, Nonlinear phonon-assisted cyclotron resonance via two-photon process in parabolic quantum well, Superlattice. Microst. 83 (2015) 755.
[53] N.D. Hien, D.V. Thuan, C.A. Duque, E. Feddi, F. Dujardin, L.T.T. Phuong, B.D. Hoi, C.V. Nguyen, L.T.N. Tu, H.V. Phuc, N.N. Hieu, One- and two-photon-induced magneto-optical properties of hyperbolic-type quantum wells, Optik 185 (2019)

1262.
[54] E. Ozturk, I. Sökmen, The effects of hydrostatic pressure on the nonlinear intersubband transitions and refractive index changes of different QW shapes, Opt. Commun. 285 (2012) 5223.
[55] F. Ungan, U. Yesilgul, E. Kasapoglu, H. Sari, I. Sökmen, The effects of hydrostatic pressure and intense laser field on the linear and nonlinear optical properties of a square quantum well, Opt. Commun. 285 (2012) 373.
[56] F. Ungan, R.L. Restrepo, M.E. Mora-Ramos, A.L. Morales, C.A. Duque, Intersubband optical absorption coefficients and refractive index changes in a graded quantum well under intense laser field: effects of hydrostatic pressure, temperature and electric field, Physica B 434 (2014) 26.
[57] D. Gammon, S. Rudin, T.L. Reinecke, D.S. Katzer, C.S. Kyono, Phonon broadening of excitons in GaAs/Al_xGa_{1-x} as quantum wells, Phys. Rev. B 51 (1995) 16785.